Journal of Solid State Chemistry **153,** 310–316 (2000)
doi:10.1006/jssc.2000.8770, available online at http://www.idealibrary.com on IDEAL®

Computer Modeling Study of the Lithium Ion Distribution in Quaternary Li–Mn–Fe–O Spinels

S. M. Woodley[1] and C. R. A. Catlow

Davy-Faraday Laboratory, The Royal Institution of Great Britain, 21 Albemarle St., London, W1X 4BS, United Kingdom

and

P. Piszora, K. Stempin, and E. Wolska

Laboratory of Magnetochemistry, Adam Mickiewicz University, Grunwaldzka 6, PL-60780 Poznan, Poland

Received February 15, 2000; in revised form May 3, 2000; accepted May 11, 2000; published online July 18, 2000

Computational and experimental techniques have been used to investigate the structural properties, especially the cation distribution, of spinel solid solutions formed between $LiMn_2O_4$ and $LiFe_5O_8$. The series of solid solutions of composition $(1-x)LiMn_2O_4-xLi_{0.5}Fe_{2.5}O_4$ are single-phase products with the cubic spinel structure, with the lattice parameter increasing from 8.21 to 8.33 Å as x varies from 0 and 1. The variation of the unit cell parameter with x shows a distinct departure from Vegard's law, which is most pronounced for samples with the Fe : Mn molar ratio close to 1 : 1. With higher Fe content, the ordering of lithium ions in the octahedral spinel sites leads to the reduction of the crystal symmetry and to a strongly marked preference of Li^+ ions to occupy the octahedral positions. Our lattice energy minimization results make clear predictions as to the Li^+ ion content and distribution in these materials and thereby resolve confusions in the experimental data.

Key Words: **computer modeling; crystal structure refinement; interatomic potentials; energy minimization.**

1. INTRODUCTION

The system $(1-x)LiMn_2O_4$–$xLi_{0.5}Fe_{2.5}O_4$ forms a continuous series of solid solutions with x varying from 0 to 1. In the stoichiometric cubic spinel $LiMn_2O_4$ ($x = 0$), the Li^+ ions occupy the tetrahedral 8*a* sites, with a 1 : 1 mixture of Mn^{3+} and Mn^{4+} ions randomly distributed over the octahedral 16*d* positions in the spinel lattice (space group $Fd3m$) (1). Lithium ferrite, $LiFe_5O_8$ ($x = 1$), is known to occur in two crystalline forms (2). The disordered $Li_{0.5}Fe_{2.5}O_4$ has an inverse spinel structure, with Fe^{3+} at the tetrahedral 8*a* positions and a 1 : 3 mixture of Li^+ and Fe^{3+} ions at the octahedral 16*d* positions. In the "ordered spinel" form (space group $P4_132$, $P4_332$), the Fe^{3+} ions are at octahedral 12*d* and tetrahedral 8*c* sites, and the Li^+ ions occupy the octahedral 4*b* positions (3). Furthermore, as x increases in the single-phase compounds, there is a tendency for ordering of lithium in the *B* sites, which is related to the reduction of symmetry (4–6).

The cation distribution over a spinel lattice of the whole $(1-x)LiMn_2O_4$–$xLi_{0.5}Fe_{2.5}O_4$ solid solution series has been determined recently by diffraction techniques, using structure factors obtained from measurements of the integrated intensities of individual X-ray reflections (4, 5), and by structure refinement, using the Rietveld profile analysis (6). There are differences, however, in the precise determination of the Li^+ ion content per unit cell and in the distribution of lithium ions over the cationic sites of the spinel lattice, depending on the method of measurements used. In particular, analysis of diffraction data using Rietveld refinement yields Li^+ occupancies that corresponds to an excess lithium content, which is not found when the data are analysed using integrated intensities.

The differences in the apparent Li^+ occupancies obtained from powder X-ray diffraction are not unreasonable, as lithium is a poor X-ray scatterer. For this reason, the present paper describes the application of computational methods, which are based upon lattice energy calculations that employ interatomic potentials (7), to enable a comparison of structural parameters determined by X-ray diffraction and ultimately to resolve the discrepancies found in the results for the Li^+ distribution.

2. METHODS

2.1. Experimental Details

Samples of solid solutions with the composition $(1-x)LiMn_2O_4$–$xLi_{0.5}Fe_{2.5}O_4$ were prepared from mixtures

[1] To whom correspondence should be addressed. E-mail: smw@ri.ac.uk.

0022-4596/00 $35.00

of iron–manganese oxide precursors, with appropriate quantities of Li_2CO_3, by thermal treatment at 600–750°C in air, using procedures described in detail previously (4–6). Because the Fe/(Fe + Mn) molar ratio for each sample is known, we have chosen this value (X) to label the samples.

X-ray diffraction patterns of polycrystalline samples were recorded with a computerized HZG-3 (TUR-61) diffractometer, employing the Mn-filtered Fe$K\alpha$ radiation. The structural refinements were performed using the Rietveld program package GSAS (8, 9). Data from 10° to 90° (2θ) with resolution of 0.04° (2θ) were included in the calculations.

2.2. Computational Details

All calculations performed in this study employed the static lattice computer code GULP 1.2 (10–12), which is based on the Born model of the ionic lattice, and from which the structural and crystal properties may be calculated using standard static lattice procedures. The calculation of the lattice energy is split into two parts: the long-range electrostatic term and the short-range interactions. For the latter, it is sufficient to sum in real space with a 25 Å cutoff. However, for the electrostatic part, which converges slowly, the Ewald summation (13,14) is employed which transforms the summation into two rapidly convergent series: one in real space, and one in reciprocal space. The resulting lattice energy is minimized with respect to both cell dimensions and atomic coordinates using a Newton–Raphson procedure together with the BFGS method (15) of updating the Hessian.

The short-range interactions are described using the standard pairwise Buckingham potential:

$$V(r) = A \exp(-r/\rho) - Cr^{-6},$$

(where r is the distance between ions) together with the shell model (16), where a free ion is described as a point charge coupled with a force constant k to a massless shell with charge Y in order to generate an ionic polarization of Y^2/k. The parameters A, ρ, C, k, and Y are derived using empirical fitting procedures, as will be discussed in greater detail in Section 3.

An important feature of the system studied here is that several sites show partial occupancies. In order to handle this problem, we have used a mean field theory whereby each site experiences a potential that is the average of all possible configurations on the disordered positions as discussed by Gale (11). This approach is considerably simpler than the alternative of modelling a large supercell, although we should point out that this simplicity comes at the expense of an acceptable loss in accuracy in the calculations.

3. RESULTS AND DISCUSSION

Observed, calculated, and difference profiles, resulting from the Rietveld refinement of X-ray powder diffraction data of the $Li_{1-0.5x}Fe_{2.5x}Mn_{2-2x}O_4$ series, for samples with $X = 0$, 0.7, and 1.0, are presented in Fig. 1a, 1b, and 1c, respectively. The X-ray diffraction patterns of these samples reveal the main reflections characteristic of the spinel-type

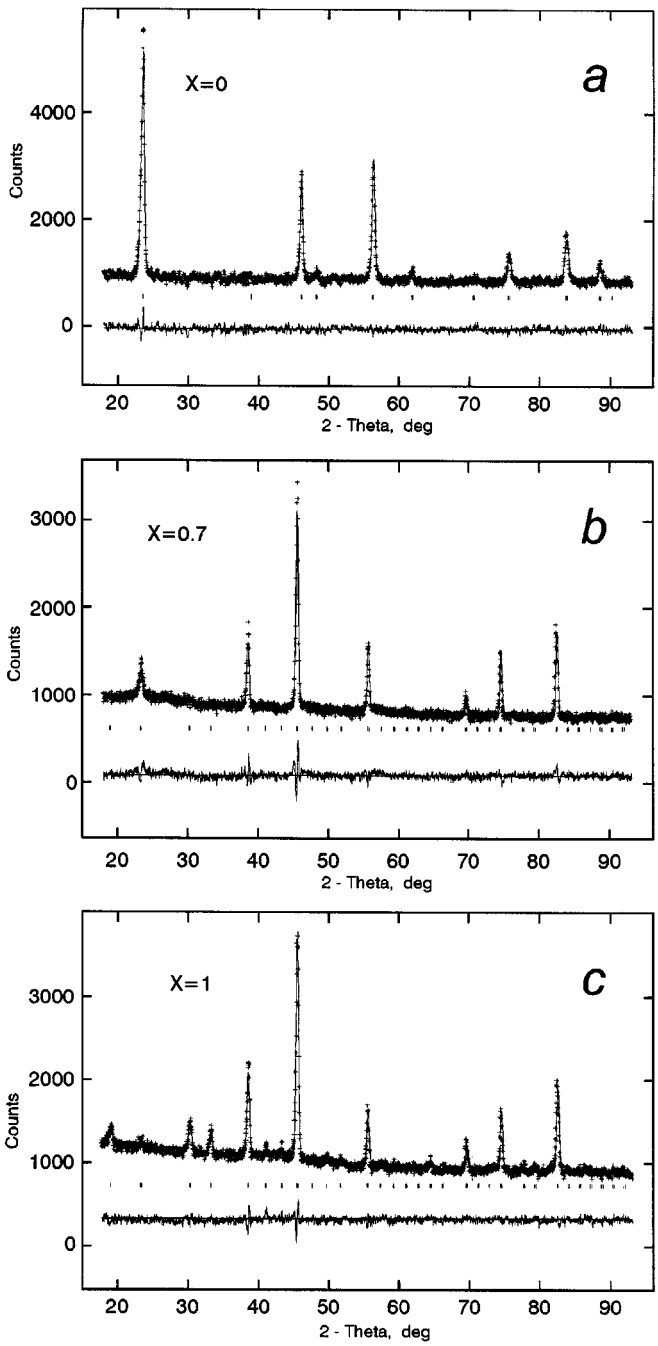

FIG. 1. Observed, calculated, and difference profiles, resulting from the Rietveld analysis of X-ray powder diffraction data collected on the $(1-x)LiMn_2O_4$–$xLi_{0.5}Fe_{2.5}O_4$ samples, with $X = 0.0$, 0.7, and 1.0.

TABLE 1
Structural Parameters for $(1-x)LiMn_2O_4$–$xLi_{0.5}Fe_{2.5}O_4$, with $0 \le x \le 0.545$, from the Rietveld Refinement in the *Fd3m* Space Group

		Coordinates	Occupancy determined for sample with						
Ion	Site	$(x = y = z)$	$X = 0.0$	$X = 0.1$	$X = 0.2$	$X = 0.3$	$X = 0.4$	$X = 0.5$	$X = 0.6$
Li^+ (A)	8*a*	0	1.00(9)	0.965(3)	0.970(4)	0.950(4)	0.679(4)	0.504(4)	0.399(3)
Fe^{3+} (A)	8*a*	0	–	0.035(7)	0.031(7)	0.050(8)	0.318(8)	0.496(7)	0.601(6)
$Li^+(B)$	16*d*	0.625	0.203(18)	0.068(2)	0.021(2)	0.025(2)	0.017(2)	0.098(2)	0.144(1)
$Fe^{3+}(B)$	16*d*	0.625	–	0.077(3)	0.184(4)	0.275(4)	0.297(4)	0.327(4)	0.396(3)
$Mn^{3+}(B)$	16*d*	0.625	0.398(9)	0.255	0.2825	0.200	0.4735	0.3757	0.2722
$Mn^{4+}(B)$	16*d*	0.625	0.398(9)	0.600	0.5125	0.500	0.2125	0.2000	0.1875
a (Å)			8.2164(4)	8.22140(31)	8.23567(27)	8.24888(25)	8.32125(26)	8.31220(27)	8.31680(30)
U			0.3883(4)	0.3875(5)	0.3873(6)	0.3880(5)	0.3884(5)	0.3891(5)	0.3909(5)
R_{wp}			7.18%	6.76%	6.85%	5.91%	6.04%	5.62%	4.79%
R_p			5.20%	4.67%	4.40%	4.12%	4.00%	3.91%	3.63%
B_{iso} $(B_{Li} = B_{Mn} = B_{Fe} = B_O)$ 1.97 Å^2									

structure. A decrease of the intensity ratio of I_{111}/I_{311} lines indicates the removal of lithium ions from tetrahedral to octahedral sites, i.e., the transformation of a normal spinel ($LiMn_2O_4$) into an inverse spinel ($LiFe_5O_8$), with the increase of Fe^{3+} content. The additional reflections (110, 210, 211, 221), visible on the X-ray pattern of sample with $X = 1.0$, are due to the 1 : 3 ordering of lithium cations in octahedral positions, resulting in the reduction of the crystal symmetry from the $Fd3m$ to the $P4_132$ ($P4_332$) space group, when the Fe/(Fe + Mn) molar ratio exceeds 0.65, that is, for $0.651 \le x \le 1.0$.

The samples investigated have been classified into two different sets referred to above. The first consists of those with molar ratio $0.0 \le X \le 0.6$, for which all reflections can be indexed according to the space group $Fd3m$. The X-ray patterns of the second set, with $0.7 \le X \le 1.0$, are characterized by the additional reflections attributed to lithium cation ordering (3), and can be assigned to the space group $P4_132$ ($P4_332$). Structural and cell parameters from the Rietveld profile refinement of both sets of X-ray powder patterns are presented in Tables 1 and 2, respectively. Changes in the interatomic distances in the AB_2O_4 spinel lattice,

TABLE 2
Structural Parameters for $(1-x)LiMn_2O_4$–$xLi_{0.5}Fe_{2.5}O_4$, with $0.65 \le x \le 1.0$, from the Rietveld Refinement in the $P4_132/P4_332$ Space Group

		Coordinates			Occupancy determined for sample with			
Atom	Site	x	y	z	$X = 0.7$	$X = 0.8$	$X = 0.9$	$X = 1.0$
$Li^+(B)$	4*b*	0.625	0.625	0.625	0.222(9)	0.270(10)	0.996(4)	0.986(29)
$Fe^{3+}(B)$	4*b*	0.625	0.625	0.625	0.435(5)	0.508(5)	0.040(4)	–
$Mn^{3+}(B)$	4*b*	0.625	0.625	0.625	0.117(7)	0.060(7)	0.060(6)	–
$Mn^{4+}(B)$	4*b*	0.625	0.625	0.625	0.231(7)	0.138(7)	0.060(6)	–
$Li^+(B)$	12*d*	0.125	0.375	− 0.125	0.172(1)	0.243(1)	–	–
$Fe^{3+}(B)$	12*d*	0.125	0.375	− 0.125	0.434(4)	0.1511(4)	0.840(1)	0.986(22)
$Mn^{3+}(B)$	12*d*	0.125	0.375	− 0.125	0.113(2)	0.082(2)	0.034(2)	–
$Mn^{4+}(B)$	12*d*	0.125	0.375	− 0.125	0.227(2)	0.160(2)	0.087(2)	–
$Li^+(A)$	8*c*	0	0	0	0.277(5)	0.152(5)	0.101(2)	–
$Fe^{3+}(A)$	8*c*	0	0	0	0.723(5)	0.848(5)	0.917(2)	0.98(16)
a(Å)					8.30591(22)	8.32825(22)	8.31084(21)	8.31438(22)
u					0.3865(5)	0.3856(6)	0.3839(6)	0.3787(9)
R_{wp}					4.57%	4.20%	4.18%	4.93%
R_p					3.54%	3.11%	3.12%	3.42%
B_{iso} $(B_{Li} = B_{Mn} = B_{Fe} = B_O)$ 1.97 Å^2								

TABLE 3
Interatomic Distances in the $(1-x)LiMn_2O_4$–$xLi_{0.5}Fe_{2.5}O_4$ Spinel Solid Solutions for $0 \le x \le 0.545$[a] (Space Group $Fd3m$)

	Bond length (Å)						
Bond	$X = 0.0$	$X = 0.1$	$X = 0.2$	$X = 0.3$	$X = 0.4$	$X = 0.5$	$X = 0.6$
A–*B*	3.4056(10)	3.40841(12)	3.41433(10)	3.41980(9)	3.44980(10)	3.44606(10)	3.44796(11)
A–O	1.978(6)	1.958(8)	1.959(8)	1.972(8)	1.995(8)	2.003(8)	2.029(7)
B–*B*	2.9043(7)	2.90670(8)	2.91175(9)	2.91642(9)	2.94200(7)	2.93881(7)	2.94043(8)
B–O	1.9452(33)	1.958(4)	1.962(4)	1.960(4)	1.975(4)	1.967(4)	1.956(4)

[a] "*A*" represents the ions on tetrahedral sites, and "*B*" represents the ions on octahedral sites.

determined by Rietveld analysis (Tables 3 and 4) are in line with the increase of lattice constants and with the decrease in the values of the oxygen u parameter.

The occupancy of manganese in 16*d* (*B*) sites, for the sample with $X = 0.0$ ($x = 0.0$), is in good agreement with the arrangement $Li[Li_{1/3}Mn_{5/3}]O_4$, in which $\frac{1}{3}$ of the Li^+ ions compensate the oxidation of Mn^{3+} to Mn^{4+} (17). In Fig. 2, the distribution of Li^+ ions over a range of sites is given together with the total lithium content, deduced from the Rietveld analysis. The increase of the Fe^{3+} content in the samples appears to be associated with a decrease of the total lithium content and with a simultaneous migration of Li^+ from tetrahedral to octahedral sites. The preference of Li^+ to occupy Wyckoff 4*b* positions is strongly marked only in samples with $X > 0.65$, although the X-ray reflections characteristic of the cubic primitive unit cell appear already for lower X values, e.g., for $X = 0.7$.

The results presented above reveal marked differences in the Li^+ distributions obtained by the two different X-ray methods, i.e., by measurements of the integrated intensities of individual X-ray lines as performed previously (4) and by the line-profile refinement with the Rietveld method (6). In particular, results for the former method for the first member of the solid solution, $LiMn_2O_4$, are consistent with the nearly stoichiometric lithium content in this sample (4,5), while from Rietveld analysis there appears to be an excess of Li^+, which may be expressed by the formula $Li_{4/3}Mn_{5/3}O_4$. These divergent results could be explained by the uncertainty in the determination of the crystallographic positions of such light atoms as lithium by X-ray diffraction techniques.

In an attempt to understand the factors affecting the cation distribution in the spinel lattice, we applied our computer modeling techniques. The procedure involved minimising the lattice energy, as explained above, for each proposed structure for the series $X = 0.0, 0.1, 0.2, \ldots, 1.0$ and investigating how the Li^+, Fe^{3+}, Mn^{3+}, and Mn^{4+} ion distributions on the octahedral sites affected the lattice parameters. For each sample we modeled the spinel structure (which has no oxygen vacancies) in two different ways:

TABLE 4
Interatomic Distances in the $(1-x)LiMn_2O_4$–$xLi_{0.5}Fe_{2.5}O_4$ Spinel Solid Solutions for $0.65 \le x \le 1.0$[a] (Space Group $P4_332$)

	Bond length (Å)			
Bond	$X = 0.7$	$X = 0.8$	$X = 0.9$	$X = 1.0$
A–*B*	3.44344(8)	3.45271(8)	3.44549(7)	–
A–O	1.964(8)	1.955(8)	1.928(9)	1.854(16)
B–*B*	2.93658(5)	2.94448(6)	2.93833(5)	2.93958(6)
B–O	1.986(4)	1.998(4)	2.006(5)	2.048(9)

[a] "*A*" represents the ions on tetrahedral sites, and "*B*" represents the ions on octahedral sites.

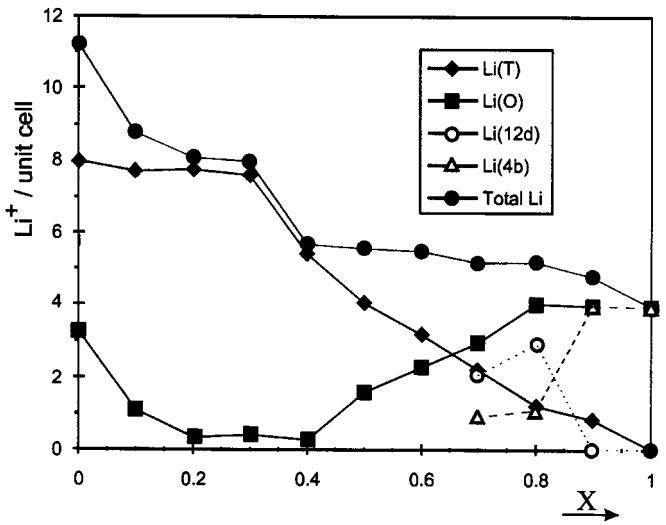

FIG. 2. Distribution of lithium ions over the spinel cationic positions, determined from Rietveld refinement, per unit cell, $A_8[B_{16}]O_{32}$. Li(T)–Li^+ in *A* (8*a*, F*d*3*m*) sites; Li(O)–Li^+ in *B* (16*d*, *Fd*3*m*) sites; Li (12*d*) and Li (4*b*) are the octahedral 12*d* and 4*b* sites of $P4_132$ space group, respectively.

TABLE 5

Core–Shell Spring Constant k and the Charge on the Shell Y Used in the Shell Model for an Ion G and the Parameters Used in the Buckingham Potential between the O^{2-} Ion and an Ion G

G	A (eV)	ρ (Å)	C (eV Å^{-6})	Y (e)	k (eV Å^{-2})
Li_A^+	426.480	0.3000	0.00		
Li_B^+	479.837	0.3000	0.00		
Fe_A^{3+}	1240.232	0.3069	0.00	1.029	10082.50
Fe_B^{3+}	1342.754	0.3069	0.00	1.029	10082.50
Mn^{3+}	1686.125	0.2962	0.00	1.029	148.00
Mn^{4+}	3087.826	0.2642	0.00		
O^{2-}	22.41	0.6937	32.32	− 2.513	20.53

[a] The subscript A or B indicates that the respective cation is in a tetrahedral or octahedral environment.

with stoichiometric quantities ($x = 0.000$, 0.082, 0.167, 0.255, 0.348, 0.444, 0.545, 0.651, 0.762, 0.878, 1.000) and then with the cation distribution close to that predicted by our Rietveld refinement. For each value of X, the same Fe^{3+}/Li^+ molar ratio for the tetrahedral 8*c* sites was used for both sets. In order to change the lithium content on the octahedral sites, we varied the Mn^{4+}/Mn^{3+} molar ratio whilst maintaining a total charge of zero for the unit cell, full occupancies on the 8*c* and 16*d* sites (vacancies would not help us model excess Li^+) and the molar ratio Fe/(Fe + Mn) constrained to the value X.

Our initial approach was to use literature parameter values (12, 18) of A, ρ, C, k, and Y for the Li^+–O^{2-}, Fe^{3+}–O^{2-}, Mn^{4+}–O^{2-}, and O^2–O^{2-} interactions and derive parameters for the Mn^{3+}–O^{2-} term. Our criterion was the reproduction of structural parameters with $X = 1.0$ ($LiFe_5O_8$) and $X = 0.3$ ($Li_{1-0.5x}Fe_{2.5x}Mn_{2-2x}O_4$ with $x = 0.255$), the two members for which the cation distributions are known most accurately. Using our fitted potentials the lattice parameters for these compositions are reproduced to within 0.7% and 0.1%, respectively. However, when the parameters for Mn^{3+}–O^{2-} were fitted to reproduce the structure of $X = 0.3$ ($x = 0.255$), the resulting potentials produced poor lattice parameters for the binary oxide α-Mn_2O_3 with the bixbyite structure. To increase transferability (a requirement if we are to model reliably the other members of the series), we decided to refine the literature values to maximize the agreement of the lattice parameters for $X = 1.0$ and $X = 0.3$ while allowing a maximum difference in the lattice parameter of 1.6% for the binary oxides α-Fe_2O_3, γ-Fe_2O_3, β-MnO_2 (rutile structure), and α-Mn_2O_3. In order to achieve this condition, we needed to refine a different A parameter for Fe^{3+}–O^{2-} when the cation is in an octahedral rather than a tetrahedral coordinated environment and likewise with the Li^+–O^{2-} term. Our fitted parameters are given in Table 5. As expected, the A parameter for the tetrahedrally coordinated sites are smaller than the A parameter for the octahedrally coordinated sites.

The difference between the observed and calculated unit cell parameters of the binary oxides is at most 1.54%. Although the variations of the observed lattice parameter across the solid solution series we are investigating are smaller we would expect that the errors in our calculated lattice parameters are systematic and constant and as such will not affect our conclusions as to the Li^+ occupancies.

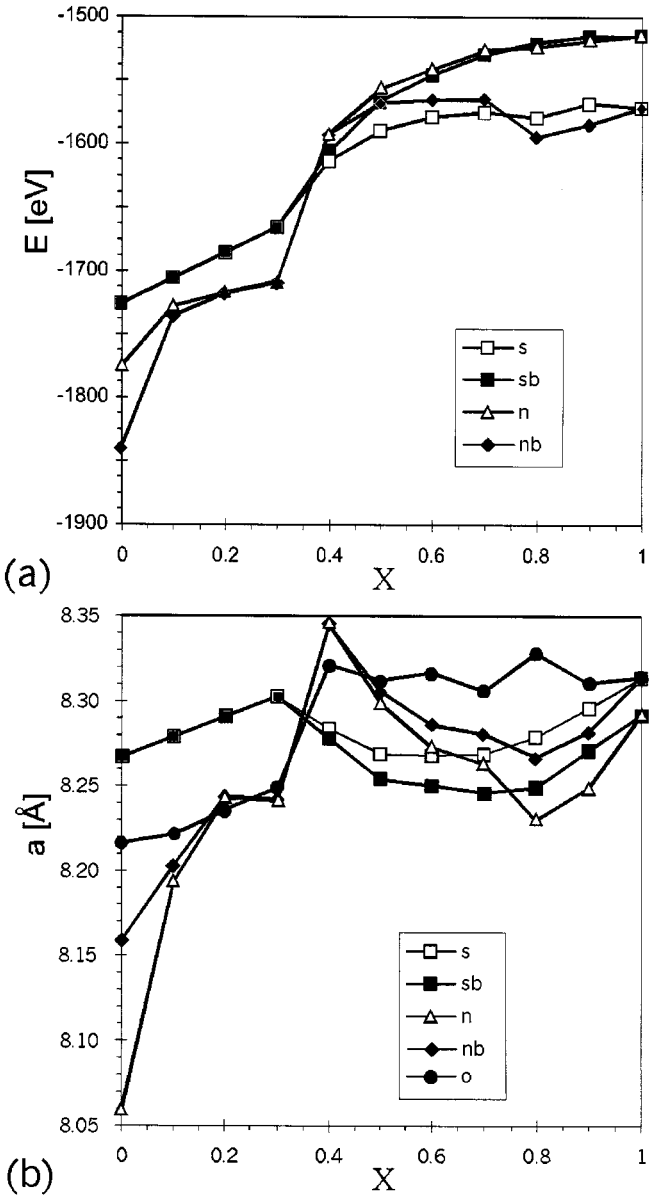

FIG. 3. (a) Lattice energy values and (b) unit cell parameters of the spinel solid solutions $(1 - x)LiMn_2O_4$–$xLi_{0.5}Fe_{2.5}O_4$ for stoichiometric (**s** and **sb**) and nonstoichiometric (**n** and **nb**) molar ratios of the cations and for that observed by X-ray diffraction data (**o**). The label **b** implies that the Li_B^+ refer the 4*b* sites.

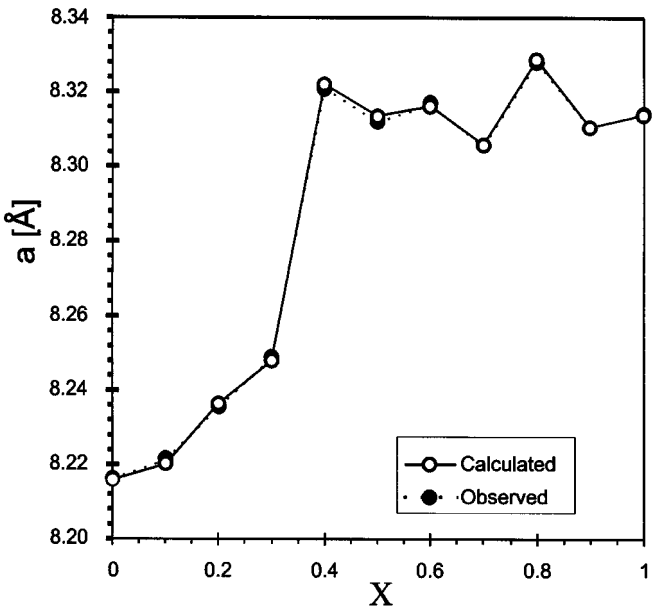

FIG. 4. Calculated unit cell parameter of the spinel solid solutions $(1-x)LiMn_2O_4$–$xLi_{0.5}Fe_{2.5}O_4$ with the Li^+ content on the 4*b* sites fitted such that the observed (from X-ray diffraction data) unit cell parameter is reproduced.

Using our refined parameters, the percentage difference in the lattice parameters for α-Fe_2O_3, γ-Fe_2O_3, β-MnO_2, Mn_2O_3, and the $(1-x)LiMn_2O_4$–$xLi_{0.5}Fe_{2.5}O_4$ solid solution with $x = 0.255$ ($X = 0.3$) and $x = 1.000$ ($X = 1.0$) are -0.11 (and -0.05), -0.51, -1.33 (and 0.32), -1.54, 0.24, and 0.00, respectively, suggesting that, as shown previously, the methods used to model the crystal structures of relatively simple binary and ternary oxides can also be adapted to complex mixed-metal compounds (19, 20) given a careful choice of interatomic potentials.

The total Li^+ content per unit cell, in samples with $0.0 \leq X \leq 0.3$, resulting from Rietveld refinement (see Fig. 2) surpasses the stoichiometric ratio (e.g., 11 Li^+ per unit cell for $X = 0.0$). As mentioned above, this finding was not confirmed by other methods (4, 5). We have calculated the lattice energy and the unit-cell parameters for systems where the lithium content is as close to that suggested by Rietveld refinement (e.g., the maximum, $10^2/_3$, Li^+ per unit cell for $X = 0.0$ was modeled) and for those with stoichiometric compositions. Our initial calculations were also performed assuming the Li^+ distributions to be both random over just the 4*b* sites and random over the 16*d* (4*b* + 12*d*) sites.

The results, shown in Fig. 3, give a good illustration of the changes in the lattice energy and the unit-cell parameter for the solid solution series. We can use this information to resolve the first of two key structural issues, the ordering of the lithium ions. Comparing the lattice energies, for the structures with the Li^+ content close to that predicted by Rietveld refinement, suggests that the lithium ions (not on the tetrahedral 8*c* sites) prefer the 4*b* sites although the energy difference drops to 0.4 eV for $X = 0.4$. This trend is perhaps clearer when comparing the lattice energies for the structures with stoichiometric Li^+ content, except for $X < 0.35$ where there are no Li^+ on the octahedral sites to distribute. For both sets, the energy difference is generally greater for higher values of X, suggesting that the Li^+ on octahedral sites for samples with higher values of X are more likely to prefer to be on 4*b* sites, in agreement with the experimental data discussed above. The lattice parameters for the lower energetic structures (in which Li^+ is not distributed on the 12*d* sites) are also closer to those observed from the X-ray diffraction data. However, upon comparing the observed and predicted lattice parameters there is still a marked difference especially for $X < 0.15$ and $X > 0.55$. Moreover, the lattice parameter is very sensitive to the lithium content.

Since the observed lattice parameter for $0 < X < 0.15$ is bounded by our calculated values for the lattice parameter, we decided to vary the lithium content on the 4*b* sites such

TABLE 6
Cation Distribution for Our Samples Resulting from Fitting the Lattice Parameter to That Observed in the X-Ray Diffraction Data

X	Li_A^+	Fe_A^{3+}	Li_B^+ 4*b*	Fe_B^{3+} 4*b*	Mn_B^{3+} 4*b*	Mn_B^{4+} 4*b*	Fe_B^{3+} 12*d*	Mn_B^{3+} 12*d*	Mn_B^{4+} 12*d*
0.0	1.000	0.000	0.18	0.0000	0.3134	0.5066	0.0000	0.3822	0.6178
0.1	0.965	0.035	0.20	0.0667	0.2575	0.4758	0.0834	0.3218	0.5947
0.2	0.970	0.030	0.110	0.1670	0.2425	0.4805	0.1877	0.2725	0.5398
0.3	0.950	0.050	0.10	0.2538	0.1846	0.4615	0.2821	0.2051	0.5128
0.4	0.679	0.321	0.15	0.2550	0.3707	0.2243	0.2999	0.4362	0.2639
0.5	0.504	0.496	0.36	0.2328	0.2778	0.1294	0.3637	0.4341	0.2022
0.6	0.399	0.601	0.45	0.2555	0.2176	0.0768	0.4646	0.3957	0.1397
0.7	0.277	0.723	0.63	0.2114	0.1182	0.0404	0.5713	0.3195	0.1092
0.8	0.152	0.848	0.70	0.2092	0.0901	0.0007	0.6972	0.3004	0.0024
0.9	0.101	0.899	0.85	0.1264	0.0186	0.0050	0.8429	0.1241	0.0330
1.0	0.000	1.000	1.00	0.0000	0.0000	0.0000	1.0000	0.0000	0.0000

that the calculated lattice parameter matched that observed from the X-ray diffraction data, as shown in Fig. 4. Again, we kept the following constraints: zero total charge within the unit cell, $Fe/(Fe + Mn) = X$, and full site occupancies. Thus, by tuning the Li^+ content so as to map the variation of the observed lattice parameter, we were able to resolve the second of the two key structural issues; the quantity of Li^+ on the 4*b* sites. The calculated cation distribution for each sample, X, is presented in Table 6. In general, when comparing our calculated data with that suggested by our Rietveld refinement, we have predicted a slight increase of the lithium content on the *B* sites. However, for $X = 0.0$ (where Rietveld suggested a content which was larger than that physically possible) and $X = 0.1$ we predicted a reduction in the lithium content on the *B* site and no change for $X = 0.3$ and $X = 1.0$ (as these were used to fit our potential parameters).

4. CONCLUSIONS

Computer modeling studies together with X-ray powder diffraction structure refinement provided an insight into the real structure of the system of solid solutions formed between the $LiMn_2O_4$ and $LiFe_5O_8$ spinel oxides. Evaluation and refinement of the M^{n+}–O^{2-} interatomic potentials, by taking into consideration the dependence on the coordination of the cations, allowed a consistent interpretation of the experimental data, but shows that the Li^+ occupancies obtained by Rietveld refinement are inaccurate. Knowing the lattice parameter of the samples and Li^+ distribution over the tetrahedral sites, it was possible to predict the Li^+ ordering and cation occupations on the octahedral spinel positions. A neutron diffraction study is planned to test our predictions.

ACKNOWLEDGMENTS

The authors thank the British–Polish Joint Research Collaboration Programme (Project WAR/992/123) for partial support of this research.

REFERENCES

1. M. M. Thackeray, W. I. F. David, P. G. Bruce, and J. B. Goodenough, *Mater. Res. Bull.* **18,** 461 (1983).
2. M. Schieber, *J. Inorg. Nucl. Chem.* **26,** 1363 (1964).
3. P. Braun, *Nature* (*London*) **170,** 1123 (1952).
4. E. Wolska, K. Stempin, and O. Krasnowska-Hobbs, *Solid State Ionics* **101,** 527 (1997).
5. E. Wolska and K. Stempin, *Mater. Sci. Forum* **278,** 618 (1998).
6. E. Wolska, P. Piszora, K. Stempin, and C. R. A. Catlow, *J. Alloys Compd.* **286,** 203 (1999).
7. C. R. A. Catlow, R. G. Bell, and J. D. Gale, *J. Mater. Chem.* **4,** 781 (1994).
8. A. C. Larsen and R. B. Von Dreele, Report No. NO-LA-U-86-748. Los Alamos National Laboratory, Los Alamos, NM 1987.
9. R. A. Young (Ed.), "The Rietveld Method." Oxford Univ. Press, Oxford, 1993.
10. J. D. Gale, *Phil. Mag. B* **73,** 3 (1996).
11. J. D. Gale, *J. Chem. Soc., Faraday Trans.* **93,** 629 (1997).
12. S. M. Woodley, P. D. Battle, J. D. Gale, and C. R. A. Catlow, *Phys. Chem. Chem. Phys.* **1,** 2535 (1999).
13. P. P. Ewald, *Ann. Phys.* **64,** 253 (1921).
14. M. P. Tosi, *Solid. St. Phys.* **16,** 1 (1964).
15. W. H. Press, S. A. Teukolsky, W. T. Vetterling, and B. P. Flannery, "Numerical Recipes," 2nd ed. Cambridge Univ. Press, Cambridge, 1992.
16. B. G. Dick and A. W. Overhauser, *Phys. Rev.* **112,** 90 (1958).
17. T. Tokada, E. Akiba, F. Izumi, and B. C. Chakoumakos, *J. Solid State Chem.* **130,** 74 (1997).
18. T. S. Bush, J. D. Gale, C. R. A. Catlow, and P. D. Battle, *J. Mater. Chem.* **4,** 831 (1994).
19. P. D. Battle, T. S. Bush, and C. R. A. Catlow, *J. Am. Chem. Soc.* **117,** 6292 (1995).
20. T. S. Bush, C. R. A. Catlow, and P. D. Battle, *J. Mater. Chem.* **5,** 1269 (1995).